

FIXED-PHASE OBSERVATIONS OF RS CANUM VENATICORUM AND BY DRACONIS SYSTEMS

JEFFREY C. HALL

Lowell Observatory, 1400 West Mars Hill Road, Flagstaff, AZ 86001

AND

JEFFREY B. WOLOVITZ

Pennsylvania State University, University Park, PA 16802

Received 1997 December 29; revised 1998 March 2

ABSTRACT

We present our data set of same-hemisphere, or *fixed-phase*, observations of five RS Canum Venaticorum and BY Draconis binaries made with the Solar-Stellar Spectrograph at Lowell Observatory. The purpose of this study is to evaluate the level of intrinsic variability in the components of these systems, and to compare it with variability arising from rotational modulation and from long-term, activity cycle-related variability. We obtain fixed-phase observations by observing tidally locked binaries with near-integral-day periods. The fixed-phase observations reveal that the intrinsic variability of the stellar hemispheres is significantly less than the variability induced by rotational modulation or by long-term, activity-cyclic evolution, but *only when several spectral features are considered in tandem*. Fixed-phase “flickering” of the stellar hemispheres is often apparent at a *higher* level than the rotational or long-term modulation in individual activity indicators. Interpretation of rotational or long-term modulation in active, late-type stars using data that do not allow quantification of the fixed-phase variability of the stars (i.e., data that do not span several rotational periods) is extremely risky.

Key words: binaries: spectroscopic — stars: activity — stars: late-type — stars: rotation

1. INTRODUCTION

In an important paper that formally defined the RS Canum Venaticorum class of chromospherically active binaries, Hall (1976) lamented the “unfortunate coincidence” that an improbably large number of RS CVn systems have orbital periods close to an integral number of days. These integral-day systems include such familiar names as AR Lac, LX Per, and Z Her. In this paper, we turn this coincidence to our advantage by specifically targeting these and other systems, to perform same-hemisphere, or *fixed-phase*, observations of cool stars. In those systems that (1) are synchronously rotating (i.e., systems in which the rotational period of the components equals or is nearly equal to P_{orb}), and (2) have an orbital period P_{orb} that is an integer or nearly so, observations spaced by P_{orb} days are observations of the same stellar hemispheres. It is therefore possible to use these systems to examine the intrinsic variability of the stellar atmospheres, without contamination by rotational modulation. The term *fixed-phase* does not imply any specific phase; it merely denotes two observations of the same hemisphere of a star at an integral number of rotational periods. Same-hemisphere observations at different phases may be compared to examine the relative variability of different phases, as well as the relative levels of variability on different timescales.

This program is part of Lowell Observatory’s Solar-Stellar Spectrograph (SSS) project, a long-term program of monitoring of variability and activity cycles in the Sun and solar-like stars, inspired in large part by the pioneering work of Olin Wilson at the Mount Wilson Observatory. In other papers, we have discussed the calibration of stellar fluxes (Hall & Lockwood 1995; Hall 1996) and the long-term (activity cycle) variability in selected program stars (Hall, Lockwood, & Gibb 1995).

The goal of the SSS fixed-phase program is to examine

the hemispheric variability in a broad sample of cool stars, and compare it with the rotational and activity cycle-related variability. We define hemispheric (or fixed-phase) variability as any significant variation in a spectral feature, such as Ca II K, on a stellar hemisphere from one rotation to the next. Observations from the Mount Wilson survey of dwarf stars (e.g., Baliunas et al. 1995), as well as our observations of active binaries (e.g., Hall & Ramsey 1992), show that such variability may be common at a level equal to or greater than the rotational signal or, in exceptional cases, the activity cycle.

In this paper, we limit ourselves to a sample of RS CVn and BY Draconis binaries that have near-integral-day periods (e.g., LX Per, with an orbital period of 8.033 days). These systems are rather well removed from the single dwarfs on the SSS and Mount Wilson surveys, and do not constitute a broad sample of cool stars, but they are excellent test cases for the science being attempted. The basic requirement for this program is to obtain repeated observations of the same hemispheres. Most of the systems on our program are synchronously rotating, so we know that the same hemispheres are visible every P_{orb} days. Additionally, these close binaries are among the most active cool stars, and their variability, short-term and otherwise, should be easily detectable. One quantitative example of such a large orbit-to-orbit variation is a pair of observations of LX Per (Hall & Ramsey 1992) made at the same phase on successive orbits, in which the H α excess emission changed by 30%. The SSS fixed-phase program is intended to assess the degree and nature of this variability in cool stars.

In § 2, we describe our targets and the method by which we have determined the amount of excess emission in their chromospherically active spectral lines (Ca II H λ 3933 and K λ 3968, H α λ 6563, and two lines of the Ca II infrared

triplet at $\lambda\lambda 8498, 8542$). In § 3, we present our results for the systems under consideration, and in § 4 we interpret our results.

2. TARGET LIST AND ANALYSIS METHOD

The targets are listed in Table 1. Data in this table are taken from the second edition catalog of chromospherically active binary stars (CABS2; Strassmeier et al. 1993), except the ephemeris for AR Lac (taken instead from Neff et al. 1989). The short-period systems are synchronous or very nearly so, having nearly equal orbital and photometric (approximately rotational) periods. One system (OU Gem) is not as closely synchronous, and long-term fixed-phase observations of this system may be contaminated by rotational modulation.

This observing program began with the renewal of the SSS project in 1992. Large gaps in the data sets in 1993 reflect the numerous instrument fixes and upgrades we were making during that time. The SSS is a dual instrument consisting of a Littrow spectrograph operating in third order that covers 3860–4000 Å (Ca II H and K) and an echelle with 70% spectral coverage from 5000 to 9000 Å. It is fed by an optical fiber from Lowell's 42 inch (1.1 m) telescope, and typically requires a 30 minute integration on a 7th magnitude star to obtain a signal-to-noise ratio (S/N) of 100 at H α .

We reduced all the data using our in-house Interactive Data Language (IDL) reduction package (Hall et al. 1994), and placed the Ca II H and K data on an absolute intensity scale using the same method we use for our survey stars (Hall & Lockwood 1995). The echelle spectra were normalized by the well-defined continuum, while the Ca II H and K spectra were normalized using the composite $B-V$ color for each system given in CABS2.

We isolated the excess emission in the Ca II H and K, H α , and Ca II infrared triplet lines using the spectral subtraction technique that has often been applied to these systems (e.g., Huenemoerder & Ramsey 1987; Hall & Ramsey 1992; Montes et al. 1996). In this procedure, we synthesize the spectrum of the binary system using the spectra of two low-activity stars shifted in radial velocity, rotationally broadened, and weighted to match the spectrum of the binary. We subtract this synthetic spectrum from the active binary spectrum, leaving the excess emission in active lines as peaks in a spectrum that is otherwise zero. An example of the subtraction technique applied to an H α spectrum of the target star KZ And is shown in Figure 1. The two reference spectra are shown by the dotted lines. They are weighted (in this case at 50% each, since KZ And consists of two K2 V stars) and subtracted from the KZ And spectrum, leaving the subtracted spectrum at bottom.

Since we normalize the continua of the original spectra to unity, the excess equivalent widths isolated by the subtrac-

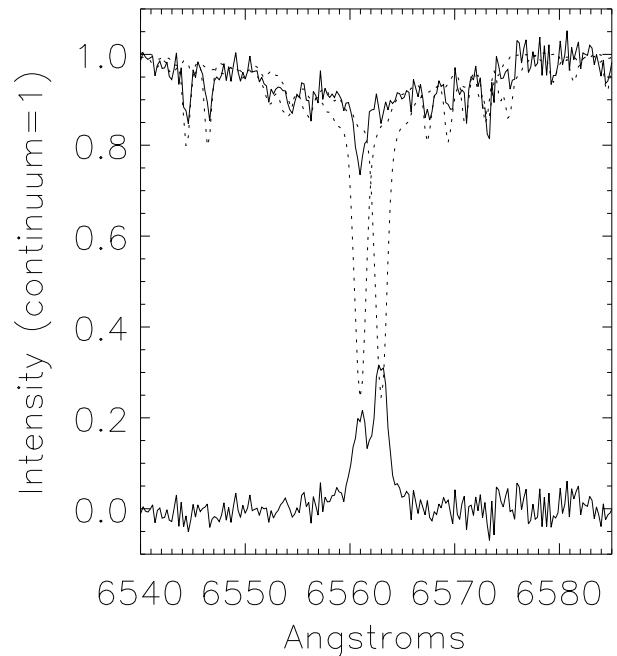


FIG. 1.—Spectral subtraction in an H α spectrum of KZ And. The KZ And spectrum is the solid line, normalized to unity. Because both components of KZ And are of the same spectral type, we have used the same star (HD 10476, K1 V) as the reference for both KZ And components. The shifted, unweighted HD 10476 spectra are shown as dotted lines. The HD 10476 spectra are each weighted equally (50%), combined, and subtracted, leaving the excess emission in KZ And visible at bottom. The rest of the order is zero, as expected in the continuum and inactive lines. The excess emission in each component of KZ And is then measured and converted to flux.

tion technique (which have units of angstroms) can be converted to excess flux densities by multiplying them by the continuum flux ($\text{ergs cm}^{-2} \text{s}^{-1} \text{\AA}^{-1}$) at the appropriate wavelength. To derive these flux densities, we used the empirical flux scales derived by Hall (1996), which express continuum fluxes as piecewise log-linear functions of common color indexes (Johnson $B-V$, $V-R$, and $R-I$, and Strömgren $b-y$). We obtained $B-V$ color indexes for each star from Table 2 of CABS2, double-checking the values in the primary references as recommended therein, and deriving individual component colors from the spectral types where necessary.

The well-known variability in color index with activity is a source of error in this procedure, as are the discrepancies between $B-V$ and the redder color indexes ($V-R$, $V-I$; Fekel, Moffett, & Henry 1986). These authors found that the excesses are probably in the red rather than in $B-V$ (see the discussion in their § 2). For this reason, we have used $B-V$ to perform the continuum normalizations and flux conversions for this paper. Fekel et al. (1986), based on

TABLE 1
BASIC PROPERTIES OF TARGET STARS

Name	Ephemeris	P_{phm} (days)	V	$B-V$	$MK_{c,h}$
KZ And	2,442,371.641 + 3.032867E	3.03	8.0	0.89	K2 V/K2 V
AR Lac	2,444,977.0216 + 1.98317E	$\approx P_{\text{orb}}$	6.1	0.72	K0 IV/G2 IV
Z Her	2,413,086.348 + 3.992801E	3.962	7.2	0.59	K0 IV/F4 V
LX Per	2,427,033.120 + 8.038207E	7.905	8.1	0.94/0.56	K0 IV/G0 V
OU Gem	2,443,846.2 + 6.991868E	7.36	6.8	0.95	K5 V/K3 V

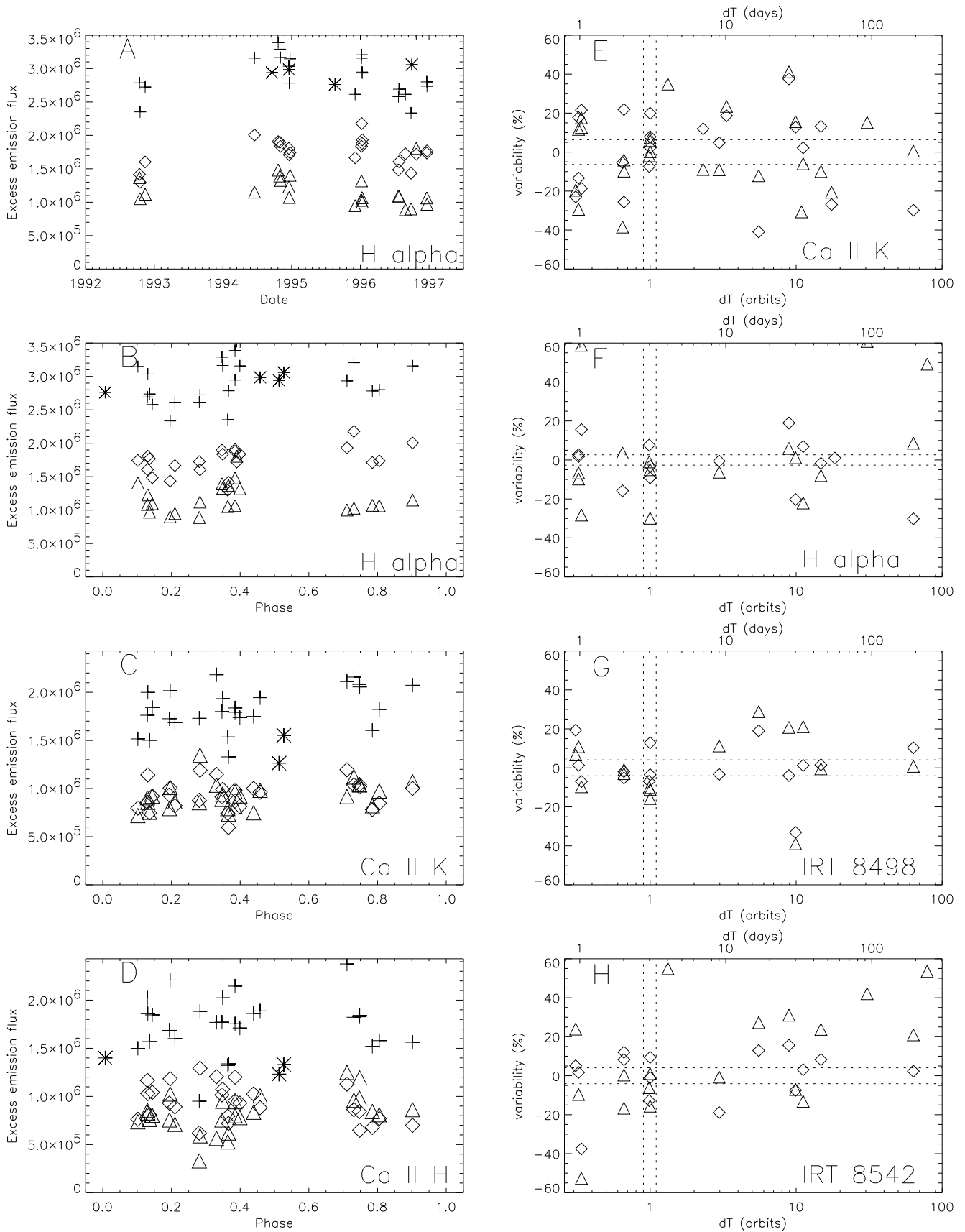


FIG. 2.—Sample results for KZ And. The left column of panels shows the excess emission flux densities (in $\text{ergs cm}^{-2} \text{s}^{-1}$) for several different lines, as indicated at lower right in each panel. Diamonds and triangles denote emission from the primary and secondary components, respectively, while plus signs indicate the total from both components. Asterisks indicate blends. In (a) the data are plotted by date; in (b–d) they are plotted by phase. The right column of panels shows the percentage variability in pairs of observations of KZ And. The time difference for each pair is shown in units of days (*top axis*) and orbits (*bottom axis*). The *x* scaling is logarithmic, to make the small- ΔT portion of the figure more visible.

TABLE 2
PERCENTAGE VARIABILITY IN FIXED-PHASE OBSERVATIONS OF TARGET STARS

SSS Frames	Average Phase	Ca K	H α	IRT λ 8498	IRT λ 8542
KZ And:					
05248/05294.....	0.137	-7.4/-1.9	7.6/-1.0	-6.9/-10.1	-12.3/-8.3
00441/00520.....	0.365	19.9/7.4	-9.2/-29.9	12.9/-15.7	10.3/-15.3
02279/02382.....	0.348	7.8/5.9	-3.2/-5.0	-3.5/-11.1	-1.3/1.4
03605/03699.....	0.748	2.3/0.2
LX Per:					
02155/02290.....	0.298	-24.7	8.7	-0.3	13.0
01093/01296.....	0.722	16.7	26.3
Z Her:					
01858/01865.....	0.057	19.3/...	.../...	.../-8.2	.../-41.5
05360/05439.....	0.136	27.5/...	65.0/32.1	-23.8/-60.9	-8.9/8.7
05225/05298.....	0.368	-52.4/...	35.4/-5.9	-1.0/30.1	3.3/46.4
04970/05058.....	0.390	-12.4/...	-45.7/21.1	27.5/-2.0	-19.9/-5.1
03602/03722.....	0.723	-9.2/...	.../...	.../...	.../...
AR Lac:					
03604/03660.....	0.125	-52.4/34.5	.../...	.../...	.../...
03660/03723.....	0.131	35.2/53.7	.../...	.../...	.../...
02108/02172.....	0.182	-0.8/18.5	.../...	-34.6/-20.6	41.9/34.6
02172/02200.....	0.190	27.0/21.7	.../...	.../...	.../...
02312/02380.....	0.200	-25.4/4.1	-1.1/-9.1	-32.9/-26.4	-0.7/-0.4
01767/01815.....	0.203	-3.6/3.1	.../...	.../...	.../...
05395/05450.....	0.214	14.9/-2.3	14.9/8.3	.../...	.../...
03227/03252.....	0.237	34.8/52.5	11.9/-10.5	15.1/17.9	-12.6/-1.8
03252/03298.....	0.255	-24.8/-78.1	.../...	10.3/5.8	6.9/41.6
03298/03403.....	0.267	7.9/19.4	51.3/2.5	.../...	.../...
04467/04526.....	0.468	0.0/12.9	.../...	.../...	.../...
03697/03755.....	0.644	-23.8/-33.9	.../...	.../...	.../...
02278/02347.....	0.697	-10.9/-55.0	.../...	-8.9/2.1	30.9/30.1
05420/05481.....	0.709	27.9/37.9	49.7/24.3	6.0/-0.4	20.1/14.8
03326/03423.....	0.766	-2.5/4.8	.../...	.../...	.../...
05127/05153.....	0.799	-24.7/-97.4	.../...	.../...	.../...
03481/03502.....	0.819	2.2/0.9	.../...	.../...	.../...
03629/03697.....	0.823	-12.5/54.8	-6.0/35.2	.../...	.../...

a private communication from B. Bopp, report a 0.02 mag change in $B-V$ from a large (30% surface coverage) spot 1000 K cooler than the surrounding photosphere. The empirical flux scales of Hall (1996) show that the log sur-

face flux varies as $-1.995(B-V)$, $-1.081(B-V)$, and $-1.330(B-V)$ for Ca H and K, H α , and the Ca II infrared triplet (IRT), respectively. If one stellar hemisphere were 30% covered by spots, and the other hemisphere pristine, we would have 9%, 5%, and 6% errors in the flux calibrations for these three lines. The errors in this extreme case are already below the variability apparent in the spectra on all timescales; with more moderate and uniformly distributed spot coverage, the flux calibration error becomes a negligible contributor to the observed variability.

TABLE 3
PERCENTAGE VARIABILITY IN TARGET STARS

Line	Total	$\Delta T < 0.9$	$0.9 < \Delta T < 1.1$	$1.1 < \Delta T$
KZ And:				
Ca K.....	17.5/14.4	18.4/17.9	9.4/3.9	20.0/15.7
H α	10.4/13.9	9.0/12.1	6.7/12.0	12.5/15.6
λ 8498.....	8.6/12.2	7.0/6.2	7.8/12.3	9.9/15.9
λ 8542.....	10.6/16.2	12.9/20.6	7.7/7.6	10.3/16.7
AR Lac:				
Ca K.....	20.3/34.0	22.3/35.7	16.8/31.1	17.2/31.2
H α	58.9/27.1	53.2/16.8	22.4/14.9	68.1/41.4
λ 8498.....	25.3/18.8	35.3/23.6	18.0/12.2	17.2/11.6
λ 8542.....	28.0/41.7	25.9/31.4	18.9/21.0	37.9/56.6
Z Her:				
Ca K.....	34.9/...	25.8/...	21.6/...	44.4/...
H α	49.4/28.6	44.1/30.5	48.7/19.7	57.2/25.9
λ 8498.....	27.3/55.5	34.0/54.1	17.4/30.1	20.0/57.0
λ 8542.....	48.2/91.4	60.4/92.2	10.4/17.3	34.9/90.5
LX Per:				
Ca K.....	22.8/...	21.4/...	20.7/...	23.9/...
H α	15.2/...	19.0/...	17.4/...	12.7/...
λ 8498.....	22.2/...	21.7/...	0.3/...	21.7/...
λ 8542.....	17.2/...	15.9/...	13.0/...	20.4/...
OU Gem:				
Ca K.....	20.8/39.2	23.5/57.4	.../...	19.4/29.4
H α	14.6/19.0	6.6/16.3	.../...	18.6/20.2
λ 8498.....	25.2/19.1	22.8/21.3	.../...	26.3/18.0
λ 8542.....	20.1/24.6	24.8/22.7	.../...	17.7/25.4

3. RESULTS

We plot our results for KZ And in Figure 2. Figures 2a and 2b show the excess emission in H α as a function of date and orbital phase, respectively. Diamonds indicate the emission from the primary component (the component nearer the observer at phase $\phi = 0.000$), triangles indicate the emission from the secondary. The plus signs show the total emission from both components. Asterisks indicate blends, showing the total emission at phases near conjunction where the contributions from the individual components could not be resolved. The plot symbols are scaled to be the same size as the error bars. The excess flux densities (Figs. 2a-2d) are in units of $\text{ergs cm}^{-2} \text{s}^{-1}$.

In Figures 2c and 2d we show the Ca II K and H data, respectively, plotted by orbital phase. These figures show why we do not include the Ca II H data in our analysis (§ 4). The two components of KZ And have similar levels of activity in H α , which is apparent in the K-line data in Figure 2c. However, there is a clear reversal in the apparent activity

level in Ca II H (Fig. 2*d*), with the primary's activity higher for $\phi \approx 0.250$, and the secondary's higher at $\phi \approx 0.750$. In both cases, the redshifted component has the larger H-line emission, a spurious result caused by blending with the emission in the nearby He line of the blueshifted component. Conjunction spectra show there is about 20% as much excess He emission as Ca H emission, and the magnitude of the activity-level reversal seen in Figure 2*d* is in agreement. This is a useful confidence check for the consistency of our subtraction procedure from spectrum to spectrum: here we have an expected effect, and it has emerged at the expected level over a data set of some 30 spectra.

In Figures 2*e*–2*h* we show the variability present in our KZ And data set. Each figure is scaled in days (*top axis*) as well as orbits (*bottom axis*). The *x*-axes are scaled logarithmically to expand the short-term region for clarity. The data points in each of these figures show the percentage variability in the excess emission fluxes between every pair of observations [i.e., for our N observations, we plot $(\mathcal{F}_i - \mathcal{F}_{i-1})/\mathcal{F}_i$, $i = 2, \dots, N$] that we have made of KZ And. We determined the error in each of our spectra from the noise in the subtracted continuum, and the horizontal dotted lines indicate the mean error over our entire data set for each spectral feature. Since all our observations of each target were made with the same instrument and with comparable integration times, the S/N of the different spectra is consistent to within $\approx 20\%$. The horizontal lines, therefore, approximately delineate the regions in the *y*-direction in which variability in our data may be considered statistically significant.

Each figure also has two vertical dotted lines that lie at 0.9 orbits and 1.1 orbits. These lines delineate the three timescales of variability we are studying. The region shortward of $\Delta T = 0.9$ orbits is the rotational modulation region. For KZ And ($P_{\text{orb}} = 3.03$ days), this area is populated by observations separated by 1 or 2 days. It provides a snapshot of the complete, presumably inhomogeneous surfaces of the KZ And components.

Between the dotted lines lie the true fixed-phase data: variability in a pair of observations spaced 3 days apart. Here we compare the same stellar hemispheres at successive orbits.

Finally, to the right of $\Delta T = 1.1$ orbits is the long-term variability region. There are data points points out to $\Delta T \approx 90$ orbits, arising from the long interval between the end of one KZ And observing season and the start of the next. In this region we expect to see not only rotational modulation, but longer-term effects arising from changes in the stars' overall activity levels, as well as from longitudinal drift of active regions.

We generated a set of results analogous to those plotted in Figure 2 for each system on our program, and have summarized these results in two tables. In Table 2, we show all pairs of successive-orbit observations of the systems on our program. We have tabulated the variability in every pair of observations (given by the SSS frame numbers in the first column) separated by approximately one orbit. The average phase of the two observations is given in the second column, while the remaining columns list the percentage change in excess line emission between the two observations for the primary component (before the slash) and the secondary component (after the slash). Missing entries appear where the data were of poor quality or absent altogether. (In the case of AR Lac, for example, a number of the obser-

vation pairs were taken while our echelle system was temporarily inoperative because of a problem with the CCD cooling system; thus, the H α and IRT data are sparser than the Ca K data.) We also have omitted data where the emission from the two components is blended, as the variability of the individual components at these phases is obscured.

In Table 3, we have calculated the variability between all pairs of observations for four different cases: (1) the total data set, (2) observations spaced by $\Delta T < 0.9$ orbits, (3) observations for which $0.9 \text{ orbits} < \Delta T < 1.1 \text{ orbits}$, and (4) observations spaced by $\Delta T > 1.1$ orbits. Cases 2, 3, and 4 show the variability in the system on the three timescales of interest, while case 1 serves as a fiducial.

We obtained the numbers in Table 3 as follows: For each system, in each case above, we have a set of N spectra, $\mathcal{S}_{i=1, \dots, N}$. We therefore have $N - 1$ pairs of observations, $[\mathcal{S}_i, \mathcal{S}_{i-1}]$, $i = 2, \dots, N$, separated by some time interval $\Delta T = t_i - t_{i-1}$. We define the “variability” in one of these pairs of observations as the difference in the excess flux between the two observations in the pair, $(\mathcal{F}_i - \mathcal{F}_{i-1})/\mathcal{F}_i$. The numbers in the second through fifth columns of Table 3 show the *average* difference in excess flux for all observation pairs with ΔT in the range specified in the column headings.

4. DISCUSSION

4.1. Overview of Results

Taken as a whole, the data in Figure 2 and in Table 3 show a difference in the level of fixed-phase variability and the levels of rotational or cyclic variability. In Figures 2*e*–2*h*, each point represents the variability in percentage of the excess emission flux in a pair of fixed-phase observations. In the case of KZ And, these are observations taken 3 days apart. The points lying within $0.9 \text{ orbits} < \Delta T < 1.1 \text{ orbits}$ tend to show less variability than those in the regimes to either side. These data are presented quantitatively in the top four rows of Table 3. Here we show the average variability in excess emission between all pairs of successive observations for both binary components, for the four active lines under investigation, and on the three critical timescales. In five of the eight entries for each timescale, the fixed-phase variability is significantly ($> 1 \sigma$) less than the analogous variability on other timescales. In the other three entries, however, this is not true, and we will discuss this ambiguity in § 4.3.

In the longer-period system LX Per, activity on all timescales was similar. Owing to the system's 8 day period, it was difficult to obtain true fixed-phase observations, but in the data we did obtain, the same-hemisphere variations in LX Per were comparable to those present on both the $\Delta T < 0.9$ and $\Delta T > 1.1$ orbit timescales.

We included OU Gem in the program to serve as a counterexample to the tidally locked systems discussed above. The photometric period in this system differs from the rotational period (see Table 1), so this is an example of a system where we expect fixed-phase observations to be contaminated by rotational effects. Unfortunately, the 7 day period of OU Gem prevented us from obtaining true same-hemisphere observations at successive orbits, so we cannot comment on its fixed-phase variability in this paper.

In Figure 3, we display some of the data in Table 3. Each panel of this figure shows the variability in the primary or secondary components' excess emission in the Ca K line or

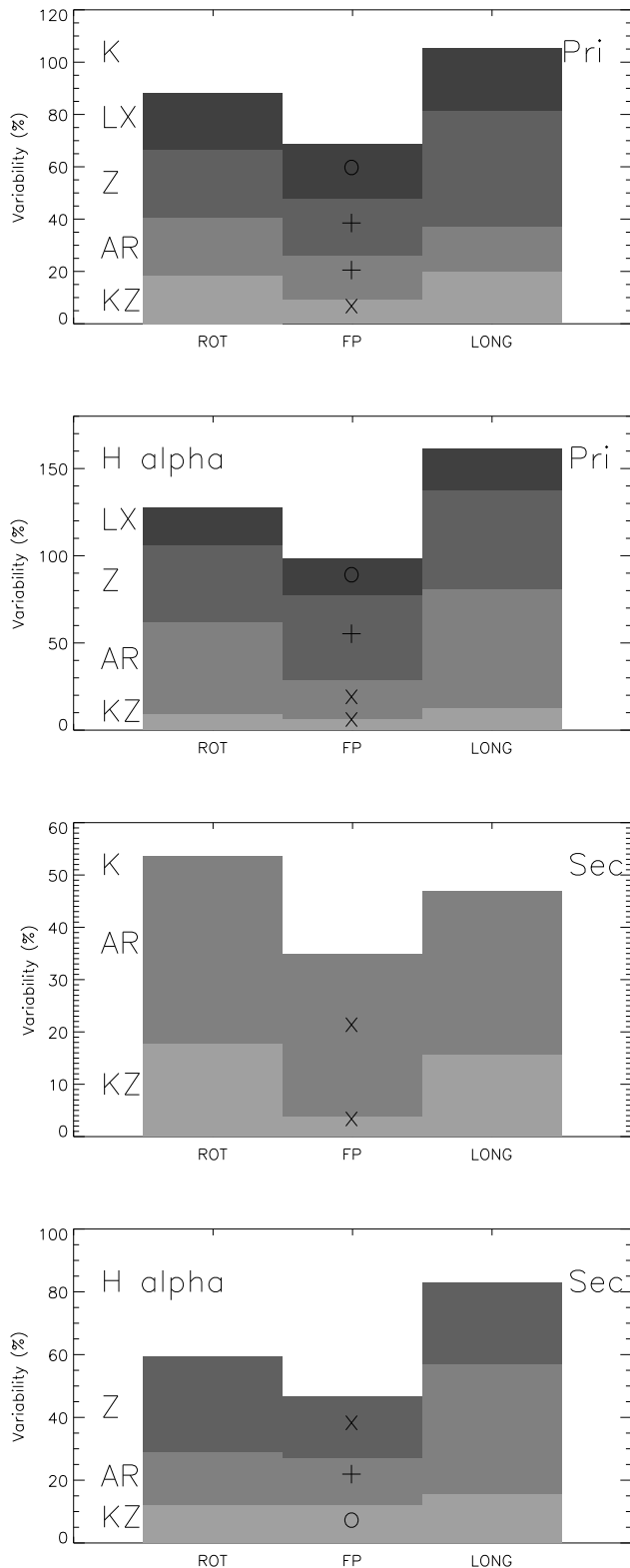


FIG. 3.—Some of the data from Table 3. Each panel shows the variability in our program stars on rotational (“ROT”), fixed-phase (“FP”), and long-term (“LONG”) timescales. The four shades of gray denote variability in KZ And, AR Lac, Z Her, LX Per (the systems’ identifying letters are shown at left). The four panels show the results for two lines (K and $H\alpha$, indicated at top left), and for primary and secondary components (indicated at top right). The results for each timescale in each system have been stacked, so the vertical scaling is arbitrary. For example, the rotational variability in the K-line of the K star in LX Per is $\approx 23\%$, not 88%.

in $H\alpha$. The results for the four tidally locked systems are stacked in each plot, so the vertical scaling is arbitrary. The horizontal axis is scaled in terms of the three timescales of interest (rotational, fixed-phase, and long-term). The decreased variability in the fixed-phase observations is obvious. A cross in a box indicates fixed-phase variability more than 1σ lower than *both* the rotational and long-term variability, while a plus sign indicates fixed-phase variability lower than that of only one of these timescales. Six boxes merit a cross, four a plus sign, and three a circle, which indicates no significant difference in variability on any of the three timescales.

The conclusion of our discussion so far is as follows: there is a clear difference between fixed-phase variability and variability on other timescales, when we consider our four binaries as an ensemble of similar stars (as in Fig. 3), or when we examine the variability for a single system across a variety of spectral features. To add some quantitative muscle to this conclusion, we determined the statistical significance of these results, as described in the next section.

4.2. Statistical Significance of Results

For each star (i.e., the 10 components of the five binaries), we have four measurements of variability (one each for Ca K, $H\alpha$, and the two IRT lines). The quantities in the second column of Table 3 give the observed variability, in each of these lines, for *all pairs* of successive observations for a given star. These values are the total envelope of variability exhibited by the star.

We wished to know whether the four measures of variability for each star on each timescale were statistically distinguishable from the four measures of overall variability of the star. After examination of the statistical methods available, we decided that a Kolmogorov-Smirnov (K-S) test (described, e.g., by Press et al. 1989), was best suited for this purpose.

For each star, we generated a random, normally distributed set of four data points having a mean and standard deviation equal to those of the data in the second column of Table 3. We tested the data on each of the three critical timescales against these randomly generated data (which mimic the overall variability of the star), using a two-sided K-S test to accept or reject the null hypothesis (H_0) that both data sets belong to the same sample. Acceptance of this hypothesis would indicate that the rotational, fixed-phase, or long-term variability of the star was indistinguishable from the variability on all three timescales combined. To compensate for the small number of data points available (three or four), we repeated this procedure 500 times for each star on each timescale, using the averaged K-S test statistic to evaluate the significance of the result.

The results are presented in Table 4. Numbers in this table indicate the confidence level at which we rejected H_0 . There were no data to test for the OU Gem fixed-phase

TABLE 4
SIGNIFICANCE OF VARIABILITY (PERCENTILE) IN TARGET STARS

System	$\Delta T < 0.9$	$0.9 < \Delta T < 1.1$	$1.1 < \Delta T$
KZ And	a/a	>99/>99	a/>99
AR Lac	a/a	>99/ ≈ 95	a/a
Z Her	a/a	≈ 98 / >99	a/a
LX Per	a	a	a
OU Gem	a/a	No data	a/a

timescale, and entries of “a” mean that H_0 was accepted for that test. Therefore, all “a” entries are those for which the level of variability in the specified subset was statistically the same as that from the random sample mimicking the star’s overall variability. Results for primary and secondary components are separated by a slash.

The null hypothesis is strongly rejected in the fixed-phase data for KZ And, AR Lac, and Z Her. The K-S test statistic T was larger for the LX Per fixed-phase data ($T = 0.541$) than for the rotational or long-term data ($T = 0.415$ and 0.431), but 0.541 was not sufficient to reject H_0 at a significant confidence level.

Of some surprise was the strong rejection of H_0 for the long-term data of the KZ And secondary. This appears to stem from the very similar level of variability in the four lines for this star (15.7%, 15.6%, 15.9%, and 16.7%) on long timescales; the larger standard deviation of the overall data set produced random data that frequently had points very different from those of the data being tested. Since this is just what the K-S test responds to, a strong positive result appeared for these data.

The conclusion of this test is that same-hemisphere observations of the stars in question exhibit significantly different levels of variability than observations on either longer or shorter timescales, and in most cases, this variability is lower than the rotational or long-term variability present. It is critical, however, to realize that this conclusion stems from the evaluation of four activity-diagnostic lines taken together. A completely different conclusion arises from investigation of these systems using individual lines, as discussed in the next section.

4.3. On the Danger of Using a Single Activity Indicator

The fixed-phase data provide an estimate of the degree of “flickering” in the chromospheres. Whether arising from global variations in the network, microflaring, or the evolution of highly transient active regions, this variability imparts noise to the rotational or activity-cyclic signal present in these stars. Our present data set, though limited to a small sample, indicates that results based on analysis of a single activity indicator such as Ca K or H α may be at best inconclusive and at worst completely misleading.

Consider KZ And. Clearly the fixed-phase variability is lower than the rotational or long-term variability, but this is only obvious when the data for all four lines being investigated are combined. From an H α study of KZ And, one would be unable to discriminate between rotational modulation and same-hemisphere variability. A K-line survey would yield better results, but even there, we find 9.0% fixed-phase variability contaminating the 18.4% rotational modulation—an S/N of 2!

But before praising Ca K too highly, consider AR Lac. Here we find 16.8% and 31.1% fixed-phase variability for the K and G star, respectively, and long-term variability of 17.2% and 31.2%. Similar results are found for the rotational data. Our 4 yr K-line record for the G star of AR Lac is flat, but this cannot be used to claim the absence of an activity cycle, since the fixed-phase “noise” would obscure a cyclic excursion of as much as 10%–15%.

The implications of this variability for techniques such as Doppler imaging are unclear, since our results are limited to four rather hyperactive chromospheric lines. We do not know (yet) what the level of fixed-phase variability is in photospheric lines. However, rotational modulation studies

using upper atmospheric lines exist (e.g., Neff et al. 1989, who used modulation of UV lines from *IUE* data to map active regions on AR Lac). Our results do not refute these authors’ interpretation of their data. Interpreting variability of, say, 25% during a single rotation of AR Lac as revealing the spatial distribution of active regions may be right on target; there are several fixed-phase data pairs in Table 2 with minimal variability (see, e.g., SSS frames 01767/01815 and 04467/04526). But there are also many observation pairs where the hemispheric flickering would either dilute or entirely obscure the nature and distribution of active regions.

It would be possible to examine true rotational modulation in data over a limited time span if some phases were demonstrably quieter than others. Our data set makes this option seem untenable. We examined the data in the second through fifth columns of Table 2 as functions of both time and phase. We found no correlation of the fixed-phase variability with either of these quantities, and significant fixed-phase variability is present at all phases.

From the results obtained in this study, therefore, we argue that interpretation of the extent and distribution of active regions on the surfaces of active, late-type stars, using a chromospheric activity indicator such as H α or Ca K, *cannot be trusted unless data for several orbital cycles are incorporated*. Only then can the intrinsic variability of the stars be established. This intrinsic variability frequently equals or exceeds the rotational or long-term variability; therefore, any rotational modulation or activity-cycle investigation that does not thoroughly evaluate it may reach conclusions that are either compromised or simply incorrect.

5. CONCLUSION

This investigation has yielded the following results:

1. The overall level of fixed-phase, hemispheric “flickering” in four RS Canum Venaticorum and BY Draconis systems ranges between 7% and 30%.
2. The fixed-phase variability in KZ And, AR Lac, and Z Her is significantly lower than the rotational and long-term variability, but this is only apparent when the results for four lines (Ca K, H α , and the Ca II IRT lines at 8498 and 8542 Å) are combined and interpreted statistically.
3. The fixed-phase variability in individual active lines often equals or exceeds the rotational and long-term variability in all systems studied. Interpretation of rotational modulation or activity cycles in the context of a single activity indicator is highly suspect unless (1) data from several orbital periods are incorporated and (2) the intrinsic variability of the stars is quantified and included in the analysis.

These results have prompted us to downgrade Ca K and H α as indicators of long-term stellar activity, though we still monitor them and recognize their importance in certain applications. A multiline approach is a better way to examine the true behavior of the star; we have initiated this work in our latest solar results (Hall & Lockwood 1998), and will develop it in forthcoming papers. We will apply it to the solar-like stars on our program with known $v \sin i$, as well as to selected binary systems, to ensure that the results presented in this paper remain unchanged on longer timescales.

We acknowledge support for this work through NSF grant ATM 94-20044. J. B. W. acknowledges assistance from the Pennsylvania State University Eberly College of Science Cooperative Education Program. We acknowledge all the Solar-Stellar Spectrograph observers who have

obtained some of the data presented in this paper: G. W. Lockwood (Lowell Observatory), Brian Skiff (Lowell Observatory), Derek Buzasi (Valdosta State University), Alastair Gunn (Jodrell Bank), and Erika Gibb (Rensselaer Polytechnic Institute).

REFERENCES

- Baliunas, S. L., et al. 1995, *ApJ*, 438, 269
 Fekel, F. C., Moffett, T. J., & Henry, G. W. 1986, *ApJS*, 60, 551
 Hall, D. S. 1976, in *IAU Colloq. 29, Multiple Periodic Variable Stars*, ed. W. S. Fitch (Dordrecht: Reidel), 287
 Hall, J. C. 1996, *PASP*, 308, 313
 Hall, J. C., Fulton, E. E., Huenemoerder, D. P., Welty, A. D., & Neff, J. E. 1994, *PASP*, 106, 315
 Hall, J. C., & Lockwood, G. W. 1995, *ApJ*, 438, 404
 ———, 1998, *ApJ*, 493, 494
 Hall, J. C., Lockwood, G. W., & Gibb, E. L. 1995, *ApJ*, 442, 778
 Hall, J. C., & Ramsey, L. W. 1992, *AJ*, 104, 1942
 Huenemoerder, D. P., & Ramsey, L. W. 1987, *ApJ*, 319, 392
 Montes, D., Fernández-Figueroa, M. J., Cornide, M., & de Castro, E. 1996, *A&A*, 312, 221
 Neff, J. E., Walter, F. M., Rodono, M., & Linsky, J. L. 1989, *A&A*, 215, 79
 Press, W. H., Flannery, B. R., Teukolsky, S. A., & Vetterling, W. T. 1989, *Numerical Recipes* (Cambridge: Cambridge Univ. Press)
 Strassmeier, K. G., Hall, D. S., Fekel, F., & Scheck, M. 1993, *A&AS*, 100, 173 (CABS2)